

## MOLECULAR DYNAMICS STUDY OF THE EFFECT OF COOLING RATE ON THE MICROSTRUCTURAL EVOLUTION OF Zr<sub>56</sub>Co<sub>28</sub>Al<sub>16</sub> ALLOY

# Murat Celtek<sup>1\*</sup>, Unal Domekeli<sup>2</sup>

<sup>1</sup>Faculty of Education, Trakya University, 22030, Edirne, Türkiye <sup>2</sup>Dept. of Physics, Trakya University, 22030, Edirne, Türkiye \*Corresponding author: mceltek@trakya.edu.tr

#### **Abstract**

In this study, the rapid solidification process of the ternary  $Zr_{56}Co_{28}Al_{16}$  alloy has been investigated using classical molecular dynamics (MD) simulations at cooling rates of 10 K/ps, 5 K/ps, and 0.1 K/ps. To describe the interatomic interactions in the system, the embedded atom method (EAM) potential, widely used for simulations of metallic systems, has been employed. The structural analyses of the system have been performed using partial and total pair distribution functions and snapshots of the instantaneous atomic configurations, while the dynamic process has been discussed by calculating the self-diffusion coefficients. The glass transition temperature ( $T_g$ ) of the system has been determined using the modified Wendt-Abraham parameter, and  $T_g$  has been observed to decrease with decreasing cooling rate. It has been found that Al atoms begin to aggregate from the supercooled region in the more slowly cooled system, which has led to unexpected anomalous behaviors in the structural analyses. Unlike Zr and Co atoms, Al atoms have been found to retain a significant degree of mobility even in the glassy state.

**Keywords:** Zr<sub>56</sub>Co<sub>28</sub>Al<sub>16</sub> alloy, rapid solidification, molecular dynamics simulations, self-diffusion coefficient, glass transition temperature, aluminum aggregation

#### INTRODUCTION

Owing to their unique internal atomic arrangements, bulk metallic glasses (BMGs) exhibit a variety of exceptional properties that surpass those of their crystalline counterparts, including high specific strength, remarkable wear resistance, excellent corrosion resistance, and superior hardness [1–3]. In recent years, BMGs particularly Zr-based alloys have received considerable attention biomedical in applications, owing to their ability to form stable ZrO<sub>2</sub> passive films that provide superior corrosion resistance compared to conventional alloys, as well as their suitability for producing components such as surgical blades, pacemakers, minimally invasive surgical devices, and dental implants [4, 5]. Most amorphous metallic systems are alloyed with expensive or toxic elements, leading to high costs or safety concerns, while their development is further constrained by processing techniques, size, and limited plasticity. Consequently, designing low-cost BMGs with high glass-forming ability and excellent performance remains a central objective in the field [6, 7]. Zr-based amorphous alloys are particularly notable for their wide supercooled liquid region and high Glass-Forming Ability (GFA). This feature was systematically investigated by Inoue et al. within the Zr-Co-Al system [8]. Their work showed that the eutectic Zr<sub>56</sub>Co<sub>28</sub>Al<sub>16</sub> alloy could be cast into 18 mm rods [8, 9]. In the present study, we focused on the effects of the cooling rate on the atomic structure of the ternary Zr<sub>56</sub>Co<sub>28</sub>Al<sub>16</sub> alloy, utilizing the advantages of classical molecular dynamics (MD) simulations. To the best of our knowledge, no comprehensive classical MD simulation study on this system has been reported.

### **EXPOSITION**

The embedded-atom method (EAM) potential parameter set proposed by Zhou et al. has been used to describe the interatomic interactions within the Zr-Co-Al system [10]. According to this method the total energy of a system consisting of N atoms can be expressed as the sum of the embedding energy associated with placing each atom into the local electron density contributed by its neighbors, and the pairwise interaction energy between atoms [11, 12].

$$E_T = \frac{1}{2} \sum_{i,j,i\neq j}^{N} \varphi_{ij} \left( r_{ij} \right) + \sum_{i}^{N} F_i \left( \rho_i \right)$$
 (1)

For further details, please refer to Refs. [13– 16]. The MD simulations were performed using the open-source simulation package DL POLY 2.0 [17]. The Zr<sub>56</sub>Co<sub>28</sub>Al<sub>16</sub> system consisted of a total of 16000 atoms in a cubic box, comprising 8960 Zr, 4480 Co, and 2560 Al atoms, and periodic boundary conditions were applied in all three dimensions throughout the simulations. To eliminate crystal symmetry and achieve thermal equilibrium, the simulation box was initially maintained at 3000 K, a temperature significantly higher than the alloy's melting point, for 5 ns. Subsequently, the simulation cell was cooled from 3000 K to 200 K under the NPT ensemble using three different cooling rates of 10 K/ps, 5 K/ps, and 0.1 K/ps. Throughout all these simulations, a Nosé-Hoover thermostat was used for temperature control, and the external pressure was set to zero [18]. For statistical calculations, the positions and velocities of the system were recorded at every 50 K temperature interval, and the OVITO package was used for visualizations [19].

The temperature-dependent evolution of the total energy of the Zr<sub>56</sub>Co<sub>28</sub>Al<sub>16</sub> system, obtained from the different cooling rates during solidification, is presented in Fig. 1. The absence of any abrupt change in the

three energy curves during rapid solidification indicates that no first-order phase transition, such as crystallization, occurs; thus, the system remains stable in an amorphous structure. In the temperature regions, the three curves nearly overlap, which is indicative of the system being liquid and the atoms possessing sufficiently high mobility. However, starting from the supercooled liquid region, differences in energy values begin to emerge dependent on the cooling rate, and these differences become even more pronounced in the glassy region (please refer to the inset of the figure).

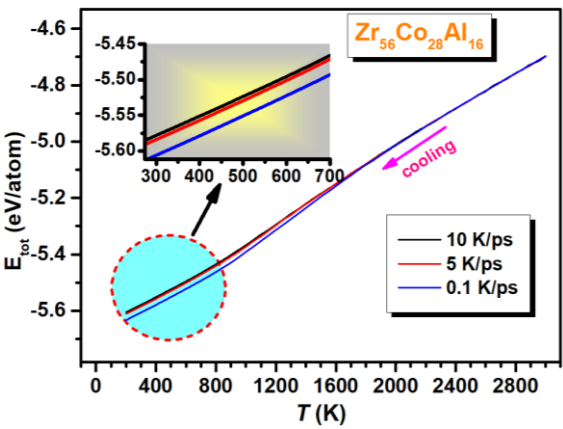


**Fig. 1.** Evolution of the system's total energy as a function of temperature for the three different cooling rates.

In MD simulation studies, one of the most preferred and useful methods for characterizing the local structure of a system is the pair distribution function (PDF). The partial PDF (pPDF or  $g_{ij}(r)$ ), which reveals atom-specific correlations, can be expressed as follows (see Ref. [20–22] for more detailed information).

$$g_{\alpha\beta}(r) = \left(\frac{V}{4\pi r^2} N_{\alpha} N_{\beta}\right) \left\langle \sum_{i}^{N} \sum_{j \neq i}^{N} \delta(r - r_{ij}) \right\rangle (2)$$

Figure 2 presents a comparison of the pPDF obtained at 300 K under three different cooling rates. The pPDF curves corresponding to the Zr–Zr, Zr–Co, and Co–Co pairs are not significantly affected by the cooling rate, except for minor variations

observed in the peak heights. That is, as the cooling rate decreases, only a slight increase is observed in the first and second peak heights of these pairs. Moreover, a splitting comprising two sub-peaks is observed in their second peaks, which is a characteristic feature of systems with an amorphous structure. However, an unusual behavior is observed for the pairs (Zr-Al, Co-Al and Al-Al) containing Al. The behavior of these pairs at 10 K/ps and 5 K/ps is similar, except for minor differences. However, the pPDF curves calculated at 0.1 K/ps are markedly different from the others. Compared to the other cooling rates, the pPDF curves of the Zr-Al and Co-Al pairs calculated from the 0.1 K/ps data exhibit a sharp decrease in the heights of their first and second peaks. This indicates that only a few Al atoms are present in the first and second coordination shells of Zr and Co atoms.

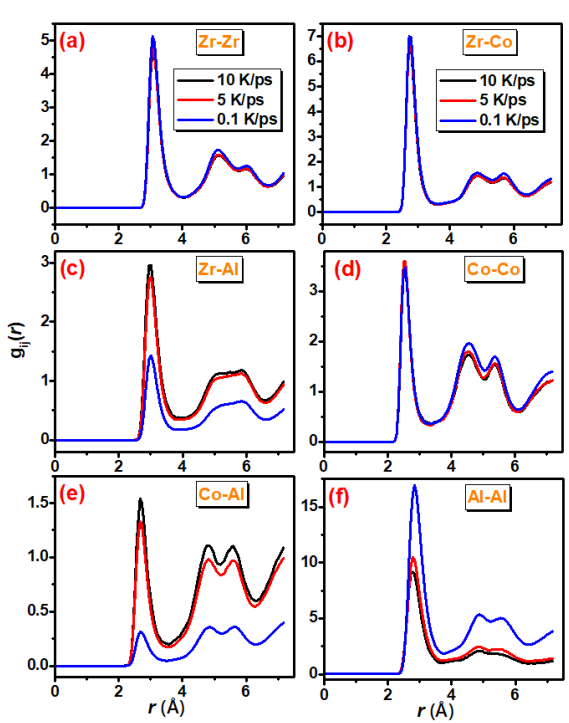


Fig. 2. Comparison of the pPDF curves for the (a) Zr–Zr, (b) Zr–Co, (c) Zr–Al, (d) Co–Co, (e) Co–Al, and (f) Al–Al pairs calculated at 300 K under three different cooling rates.

In contrast, the pPDF curves for the Al–Al pairs show the opposite trend. At a cooling rate of 0.1 K/ps, a significant increase is observed in the heights of the first and second peaks of the corresponding pPDF

curve, indicating that the first and second coordination shells of Al atoms are predominantly occupied by other Al atoms. This behavior is attributed to the aggregation of Al atoms. However, further analyses are required to examine this phenomenon more clearly.

One of the simplest and most effective ways to investigate this is by examining the instantaneous snapshots of the Zr, Co, and Al atoms in the simulation box separately (see Figure 3). As can be seen from the figure, the Zr and Co atoms are generally distributed homogeneously throughout the simulation box for all three cooling rates. However, while the Al atoms are partially dispersed throughout the simulation box at cooling rates of 10 K/ps and 5 K/ps, at 0.1 K/ps they aggregate in different regions of the box, forming large Al clusters. This sheds light on the reason behind the anomalous behavior observed in the pPDF curves of Al-containing pairs. Similar behavior of Al atoms has previously been reported in different systems [12, 23, 24].

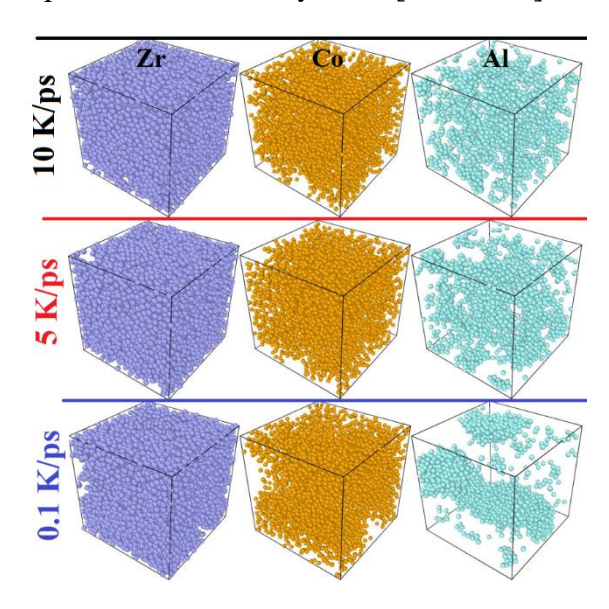
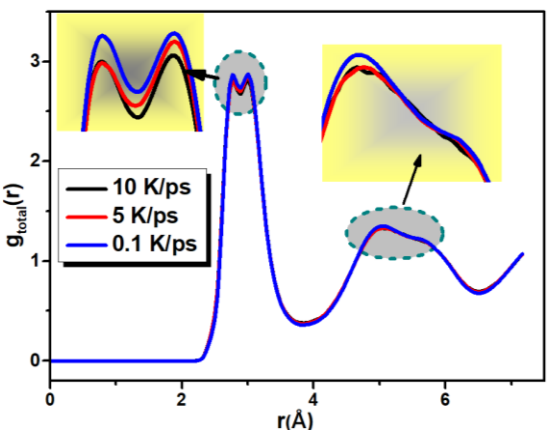


Fig. 3. Snapshots of the Zr, Co, and Al atoms in the simulation box at 300 K for the three cooling rates.

Figure 4 shows the total PDF (or  $g_{total}(r)$ ) curves at 300 K. The heights of the first and second peaks of the PDF curves increase slightly with decreasing cooling rate, but otherwise they are not significantly affected by the cooling rate (see the insets of the

figure). While these curves provide a general overview of the system as a whole, the pPDF curves offer much more detailed insights into the microscopic changes. In fact, the anomalies observed in the Al-containing pairs are not visible in the total PDF curves.



*Fig. 4.* Comparison of the total PDF curves calculated at 300 K for three different cooling rates.

To accurately describe the glass formation process during rapid solidification, it is essential to precisely determine the glass transition temperature (T<sub>g</sub>). For this purpose, the modified Wendt–Abraham (MWA or R<sup>MWA</sup>) parameter, which has been recently proposed by Celtek et al., has been used [12]. The MWA parameter is calculated using the following relation [12]:

$$R^{MWA} = \left(\frac{g_{min}}{g_{max}}\right)^2,\tag{3}$$

where  $g_{\text{min}}$  and  $g_{\text{max}}$  represent the first minimum and maximum of the PDF, respectively. As an example, the temperature dependence of the MWA parameter for the 5 K/ps cooling rate is shown in Fig. 5, while the same method was applied for the other cooling rates, and the results are presented in the insets of the figure. As shown in the figure, the intersection point of the linear fits applied to the high- and low-temperature regions has been determined as T<sub>g</sub>. Using this method, T<sub>g</sub> has been determined to be 882 K, 875 K, and 835 K for the 10 K/ps, 5 K/ps, and 0.1 K/ps cooling rates, respectively. The computed T<sub>g</sub> values are higher than the experimental  $T_g = 744 \text{ K} [25]$ . the significant considering However,

differences in simulation conditions (e.g., cooling rate or timescale) compared to the experiment, the results are deemed reasonable. In addition, the inset shows that the system's  $T_g$  decreases as the cooling rate decreases, in agreement with literature reports [26].

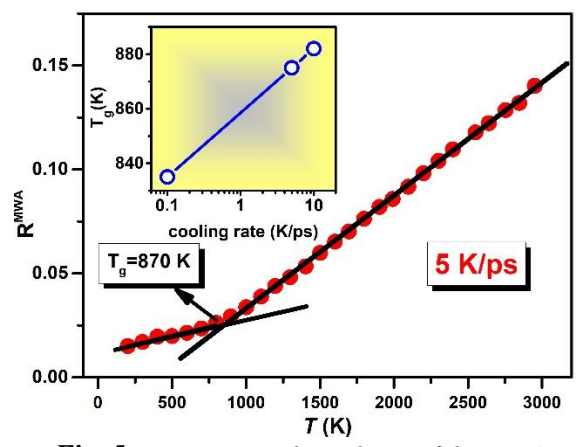


**Fig. 5.** Temperature dependence of the MWA parameter calculated for the 5 K/ps cooling rate. The inset shows the variation of  $T_g$  with cooling rate.

This section focuses on the evolution of the atomic self-diffusion coefficient (D) in the system with respect to the cooling rate across a broad temperature range. The mean square displacement (MSD) is commonly used to examine the dynamic motion of atoms, and according to Einstein's relation, the D values of atoms in the system can be calculated from the slopes of the MSD curves [27, 28].

$$D = \lim_{t \to \infty} \frac{1}{6t} \langle r^2(t) \rangle. \tag{4}$$

Figures 6(a–c) illustrate the temperature-dependent D values of Zr, Co, Al, and all atoms in the system for the three cooling rates. The temperature-dependent behavior of the D values for all three cooling rates exhibits a similar trend; that is, over a wide temperature range, Al atoms possess the highest D values, followed by Co and Zr atoms, respectively. The D values for Zr, Co, and Al atoms all decrease as the temperature is lowered. This observation is readily explained by the fact that the atoms exhibit significantly more dramatic mobility at higher temperatures compared to lower

ones. As the temperature further decreases, atomic mobility markedly reduces starting from the supercooled liquid region, and following the glass transition, atoms in the system are expected to display either highly restricted or essentially no motion. While the D values of Zr and Co atoms follow the expected trend, Al atoms deviate from this behavior, maintaining mobility even after the glass transition. Notably, at the cooling rate of 0.1 K/ps, Al exhibits a markedly different trend compared to the other elements: instead of decreasing with decreasing temperature, its D anomalously increase the in deeply supercooled region (around 1500 K). This indicates that Al atoms retain significant mobility at low temperatures and provides further insight into the Al aggregation discussed above. Figure 6(d) shows the comparison of the D values calculated for all atoms in the liquid Zr<sub>56</sub>Co<sub>28</sub>Al<sub>16</sub> system at three different cooling rates with previously reported ab-initio MD (AIMD) simulation results in the literature [29]. Overall, our findings are in good agreement with AIMD simulation results, showing only minor differences.

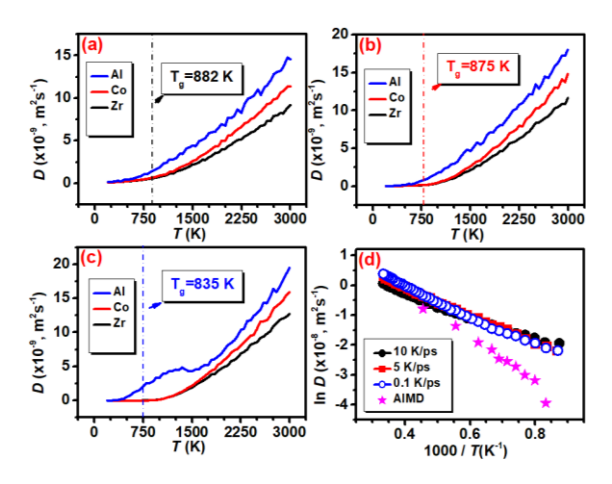


Fig. 6. Temperature dependence of the D values of Zr, Co, and Al atoms at cooling rates of (a) 10 K/ps, (b) 5 K/ps, and (c) 0.1 K/ps, and (d) comparison of the D values obtained in the liquid region with those reported from AIMD simulations in the literature.

#### **CONCLUSION**

In conclusion, the effect of cooling rate on the atomic structure and the evolution of glass formation process in the alloy during rapid Zr<sub>56</sub>Co<sub>28</sub>Al<sub>16</sub> solidification has been investigated using cooling rates of 10 K/ps, 5 K/ps, and 0.1 K/ps. The system's  $T_g$  values systematically decrease with decreasing cooling rate. The analyses revealed that as the cooling rate decreases, Al atoms tend to aggregate and exhibit atypical behavior. Moreover, the diffusion calculations reveal that Al atoms exhibit mobility at all temperatures, even within the glassy region. While the chosen EAM potential parameters generally capture the structural properties of the system effectively, a re-evaluation of the parameters specific to Al for alloys seems necessary. For future work, performing simulations with different potentials and comparing the results is recommended to obtain a more accurate and reliable description of the system.

### REFERENCE

- [1] Dong Q, Pan YJ, Tan J, et al. A comparative study of glass-forming ability, crystallization kinetics and mechanical properties of Zr55Co25Al20 and Zr52Co25Al23 bulk metallic glasses. J Alloys Compd 2019; 785: 422–428.
- [2] Han K, Qiang J, Wang Y, et al. Zr-Al-Co-Cu bulk metallic glasses for biomedical devices applications. J Alloys Compd 2017; 729: 144–149.
- [3] Löffler JF. Bulk metallic glasses. Intermetallics 2003; 11: 529–540.
- [4] Li HF, Zheng YF. Recent advances in bulk metallic glasses for biomedical applications. Acta Biomater 2016; 36: 1–20.
- [5] Liu L, Qiu CL, Chen Q, et al. Deformation behavior, corrosion resistance, and cytotoxicity of Ni-free Zr-based bulk metallic glasses. J Biomed Mater Res Part A 2008; 86A: 160–169.
- [6] Tan J, Zhang Y, Sun BA, et al. Correlation between internal states and plasticity in bulk metallic glass. Appl Phys Lett; 98. Epub ahead of print 11 April 2011. DOI: 10.1063/1.3580774.

- [7] Ashby M, Greer A. Metallic glasses as structural materials. Scr Mater 2006; 54: 321–326.
- [8] Wada T, Zhang T, Inoue A. Formation, Thermal Stability and Mechanical Properties in Zr-Al-Co Bulk Glassy Alloys. Mater Trans 2002; 43: 2843–2846.
- [9] Zhang T, Inoue A. New Glassy Zr-Al-Fe and Zr-Al-Co Alloys with a Large Supercooled Liquid Region. Mater Trans 2002; 43: 267–270.
- [10] Zhou XW, Johnson RA, Wadley HNG. Misfit-energy-increasing dislocations in vapor-deposited CoFe/NiFe multilayers. Phys Rev B 2004; 69: 144113.
- [11] Daw MS, Baskes MI. Embedded atom method: derivation and application to impurities, surfaces and other defects in metal. Phsical Rev B 1984; 29: 6443–6453.
- [12] Celtek M, Sengul S, Domekeli U, et al. Dynamical and structural properties of metallic liquid and glass Zr48Cu36Ag8Al8 alloy studied by molecular dynamics simulation. J Non Cryst Solids 2021; 566: 120890.
- [13] Celtek M, Sengul S. Effects of cooling rate on the atomic structure and glass formation process of Co90Zr10 metallic glass investigated by molecular dynamics simulations. Turkish J Phys 2019; 43: 11–25.
- [14] Celtek M. The effect of atomic concentration on the structural evolution of Zr100-xCox alloys during rapid solidification process. J Non Cryst Solids 2019; 513: 84–96.
- [15] Sengul S, Domekeli U, Celtek M. Effect of cooling rate on the atomic structure of Al75Co25 metallic glass. J Tech Univ Gabrovo 2021; 63: 76–80.
- [16] Domekeli U. A molecular dynamic study of the effects of high pressure on the structure formation of liquid metallic Ti62Cu38 alloy during rapid solidification. Comput Mater Sci 2021; 187: 110089.
- [17] Smith W, Forester TR. DL\_POLY\_2.0: A general-purpose parallel molecular dynamics simulation package. J Mol Graph 1996; 14: 136–141.
- [18] Nosé S. A unified formulation of the constant temperature molecular dynamics methods. J Chem Phys 1984; 81: 511–519.
- [19] Stukowski A. Visualization and analysis of atomistic simulation data with OVITO-the Open Visualization Tool. Model Simul

- Mater Sci Eng 2010; 18: 015012.
- [20] Celik FA. Molecular dynamics simulation of polyhedron analysis of Cu–Ag alloy under rapid quenching conditions. Phys Lett A 2014; 378: 2151–2156.
- [21] Celik FA, Kazanc S. Crystallization analysis and determination of Avrami exponents of CuAlNi alloy by molecular dynamics simulation. Phys B Condens Matter 2013; 409: 63–70.
- [22] Celtek M. An in-depth investigation of the microstructural evolution and dynamic properties of Zr77Rh23 metallic liquids and glasses: a molecular dynamics simulation study. J Appl Phys; 132. Epub ahead of print 2022. DOI: 10.1063/5.0095398.
- [23] Celtek M, Sengul S, Domekeli U. Glass formation and structural properties of Zr50Cu50-xAlx bulk metallic glasses investigated by molecular dynamics simulations. Intermetallics 2017; 84: 62–73.
- [24] Celtek M, Sengül S, Domekeli U. The Evolution of Atomic Structure of the Zr48Cu36Ag8Al8 Bulk Metallic Glass in the Rapid Cooling Process. Süleyman Demirel Univ J Nat Appl Sci 2019; 23: 954–962.
- [25] Long Y, Cao QP, Wang XL, et al. Effect of Al composition tuning on properties and structure in Zr-Co-Al metallic glass. J Alloys Compd 2022; 907: 164534.
- [26] Guder V, Celtek M, Celik FA, et al. Crystallization analysis and determination of Avrami exponents during isothermal annealing and the effect of cooling rate on the evolution of the atomic structure of Pd78Si16Cu6 alloy: A molecular dynamics simulation study. J Non Cryst Solids 2023; 602: 122067.
- [27] Celtek M. In-depth investigation of the effect of cooling rate on structural and dynamic properties of Cu54Hf46 alloy by molecular dynamics simulations. J Non Cryst Solids 2025; 664: 123615.
- [28] Domekeli U, Sengul S, Celtek M, et al. The melting mechanism in binary Pd 0.25 Ni 0.75 nanoparticles: molecular dynamics simulations. Philos Mag 2018; 98: 371–387.
- [29] Wang XL, Dong Y, Mohr M, et al. Correlation Between Viscosity and Local Atomic Structure in Liquid Zr56Co28Al16 Alloy. Microgravity Sci Technol 2022; 34: 10.